

Bayesian Estimation of the Aortic Stiffness based on Non-Invasive Computed Tomography Images

Ettore Lanzarone¹, Ferdinando Auricchio², Michele Conti², Anna Ferrara²

Second Bayesian Young Statisticians Meeting (BAYSM 2014)
Vienna, September 18–19, 2014

¹ Istituto di Matematica Applicata e Tecnologie Informatiche (IMATI),
Consiglio Nazionale delle Ricerche (CNR), Milan, Italy.
`ettore.lanzarone@cnr.it`

² Dipartimento di Ingegneria Civile e Architettura (DICAr),
Università degli Studi di Pavia, Pavia, Italy.
`<auricchio,anna.ferrara,michele.conti>@unipv.it`

Abstract

Aortic diseases are one relevant cause of death in western countries. They involve significant alterations of the aortic wall tissue, with consequent changes in the *stiffness*, i.e., the capability of the vessel to vary its section secondary to blood pressure variations. In this paper, we propose a Bayesian approach to estimate the aortic stiffness and its spatial variation, exploiting patient-specific geometrical data non-invasively derived from Computed Tomography Angiography (CTA) images. The proposed method is tested considering a real clinical case, and outcomes show good estimates and the ability to evaluate local stiffness variations. The final objective is to support the adoption of imaging techniques such as the CTA as a standard tool for early diagnosis of aortic diseases.

Keywords: ordinary differential equations; parameter estimation; aortic stiffness; descending aorta; computed tomography angiography.

1 Introduction

Arterial *stiffness*, i.e., the capability of the vessel to vary its section secondary to blood pressure variations, is a significant predictor of cardiovascular morbidity and mortality. In this scenario, this work proposes a stochastic method to assess the stiffness of a given aortic region and its spatial variation, based on non-invasively acquired information.

Aortic pressure and radius observations are linked through a constitutive model of the vessel wall, and the aortic stiffness is then estimated with a Bayesian approach [2, 7]. This methodology has already given good results in other fields, e.g., biology [1], heat transfer [5], and also biomechanics [6]; now we exploit its potentialities in this application.

2 Stiffness estimation

We consider n cross-sections of an aortic segment. Each section i (with $i = 1, \dots, n$) is assumed to be a thin-walled circular tube of isotropic linear elastic material with inner

radius r_i , thickness h_i , and Young modulus E_i . Its constitutive equation is:

$$dr_i = \frac{r_i^2(t)}{E_i h_i - P_i(t) r_i(t)} dP_i \quad (1)$$

where $r_i(t)$ and $P_i(t)$ are the state variables observed at section i over time t , whereas $E_i h_i$ is unknown. The latter is assumed as a random quantity given by a constant expected value $[E_i h_i]_0$ and a Gaussian white noise $\xi_i^E(t)$ scaled by η :

$$E_i h_i = [E_i h_i]_0 + \eta \xi_i^E(t)$$

Time t is discretized into instants t_j and state variables into values $r_{i,j} = r_i(t_j)$ and $P_{i,j} = P_i(t_j)$, respectively. Then, the discretized law is solved for $P_{i,j}$, and two further white noises are introduced, due to pressure ($\xi_{i,j}^P$) and radius ($\xi_{i,j}^r$) measurement errors. These noises are additive and proportional to $P_{i,j-1}$ and to the mean between $r_{i,j}$ and $r_{i,j-1}$, respectively. Hence, (1) is rewritten as:

$$P_{i,j} = \frac{P_{i,j-1} r_{i,j}}{2r_{i,j} - r_{i,j-1}} + \frac{[E_i h_i]_0}{r_{i,j}} \left(1 - \frac{r_i}{2r_{i,j} - r_{i,j-1}}\right) + \frac{\eta}{r_{i,j}} \left(1 - \frac{r_i}{2r_{i,j} - r_{i,j-1}}\right) \xi_{i,j}^E + \varepsilon P_{i,j-1} \xi_{i,j}^P + \psi \frac{r_{i,j} + r_{i,j-1}}{2} \xi_{i,j}^r \quad (2)$$

In this way, the conditioned density $f(P_{i,j} | P_{i,j-1}, r_{i,j}, r_{i,j-1}, [E_i h_i]_0, \eta^2, \varepsilon^2, \psi^2)$ is Gaussian, with:

$$\begin{aligned} \mu_{i,j} &= \frac{P_{i,j-1} r_{i,j}}{2r_{i,j} - r_{i,j-1}} + \frac{[E_i h_i]_0}{r_{i,j}} \left(1 - \frac{r_i}{2r_{i,j} - r_{i,j-1}}\right) \\ \sigma_{i,j}^2 &= \frac{\eta^2}{r_{i,j}^2} \left(1 - \frac{r_i}{2r_{i,j} - r_{i,j-1}}\right)^2 + \varepsilon^2 P_{i,j-1}^2 + \psi^2 \frac{(r_{i,j} + r_{i,j-1})^2}{4}. \end{aligned}$$

Given $m + 1$ observations at instants $\{t_0, \dots, t_j, \dots, t_m\}$ over the cardiac cycle, the likelihood function is:

$$f(\hat{P}_i | \hat{r}_i, [E_i h_i]_0, \eta^2, \varepsilon^2, \psi^2) = \prod_{j=1}^m f(P_{i,j} | P_{i,j-1}, r_{i,j}, r_{i,j-1}, [E_i h_i]_0, \eta^2, \varepsilon^2, \psi^2) \quad (3)$$

where \hat{P}_i and \hat{r}_i denote the respective set of observations.

Parameters to estimate are $[E_i h_i]_0 \forall i$, η^2 , ε^2 and ψ^2 . The prior densities follow the configuration usually adopted in the literature [6]:

$$\begin{aligned} g(\eta^2) &= \text{InvGamma}(\alpha_\eta, \beta_\eta) & g(\varepsilon^2) &= \text{InvGamma}(\alpha_\varepsilon, \beta_\varepsilon) \\ g(\psi^2) &= \text{InvGamma}(\alpha_\psi, \beta_\psi) & g([E_i h_i]_0 | \eta^2) &= \mathcal{N}([Eh]_0^{\text{prior}}, 2\eta^2) \end{aligned}$$

where $[Eh]_0^{\text{prior}}$ is set equal to $800 \text{ Pa} \cdot \text{m}$ to consider a Young modulus of 0.4 MPa and a wall thickness of 2 mm . As for shape and scale factors of the errors, $\alpha_\eta = 0.125$, $\beta_\eta = 0.1$, $\alpha_\varepsilon = 0.01$, $\beta_\varepsilon = 0.01$, $\alpha_\psi = 100$, and $\beta_\psi = 10$ are assumed. These choices are such that the expected value of $g(\eta^2)$ is $[Eh]_0^{\text{prior}}/10$, the expected value of $g(\varepsilon^2)$ is 10^4 , and the expected value of $g(\psi^2)$ is $10^{-3} \text{ Pa}^2/\text{m}^2$.

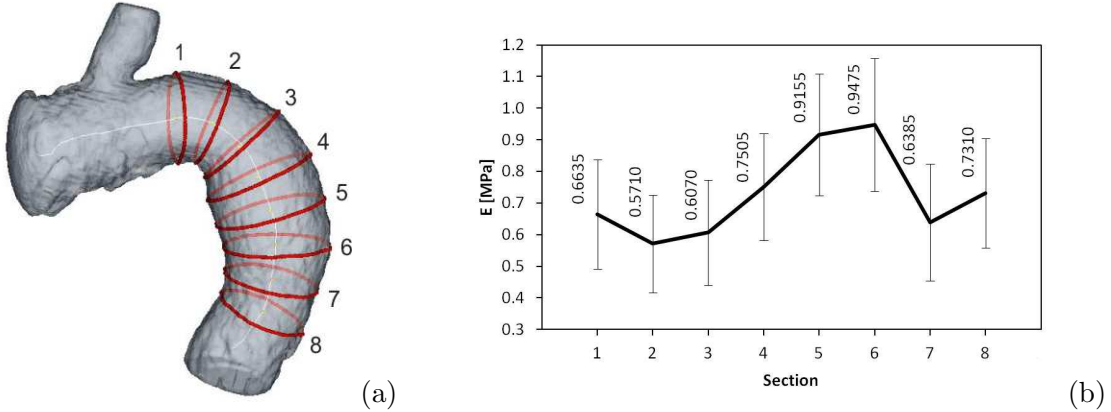


Figure 1: (a) Aorta geometric reconstruction from CTA images with the 8 considered sections; (b) Young modules E_i estimated at each section i with $h_i=2$ mm: posterior means and error bars equal to posterior standard deviations.

3 Radius and pressure dataset

Radii $r_{i,j}$ are obtained from patient-specific CTA images. Each image is analysed to get the internal vessel radii at each considered cross-section. Then, the presence of a certain number of images (20 in our case) allows to get a temporal evolution of radii along with the cycle. The adopted imaging analysis consists of the following three steps: acquisition of patient-specific medical images; segmentation and anatomical reconstruction of the lumen profile; virtual slicing of the three-dimensional reconstruction to get the mean radius at each slice. A semi-automatic segmentation process is adopted, using the open source software ITK-Snap (www.itksnap.org).

As for $P_{i,j}$, direct non-invasive measurements in central arteries are impossible and, for keeping the methodology non-invasive, they are generated using a lumped parameter model of the arterial circulation, based on [3, 4]. This consists of a set ordinary differential equations for blood pressure and flow in different arterial segments. Numerically solving the equations, the temporal evolution of pressure in each segment is obtained, and values at the instants of CTA images are taken.

4 Results and conclusions

The proposed approach is applied to a real clinical case, considering an old female patient with a descending aorta dilation, probably related to an aneurysm, which suggests a localised vessel stiffening. Eight cross-sections in the descending aorta are taken, and peripheral resistances of the lumped parameter model are increased by 40% with respect to [3, 4] for considering patient's hypertension. Data are reported in Table 1.

Estimates are obtained in JAGS [9] with 200,000 iterations, a burn-in of 10,000 iterations, and a thinning interval of 10. Satisfactory traceplots are obtained, thus verifying the convergence of the model.

Young modules are derived assuming $h_i = 2$ mm $\forall i$; values are plotted in Figure 1. Results show good estimates in accordance with the literature [8] and with other deterministic techniques applied to get model parameters. Moreover, the stiffness spatial variation is caught, in agreement with the characteristics of the considered clinical case where a localised stiffening is expected in some sections. Computational times for obtaining estimates once CTA images are stored, including time for dataset generation, are

Time %	Sect. 1	Sect. 2	Sect. 3	Sect. 4	Sect. 5	Sect. 6	Sect. 7	Sect. 8
Cross-sectional radii from CTA images [mm]								
0	12.91	12.77	13.95	15.37	15.43	14.41	12.87	12.46
5	13.16	12.97	14.10	15.55	15.68	14.43	12.95	12.61
10	13.31	13.18	14.54	15.76	15.89	14.54	13.20	12.76
15	13.36	13.35	14.57	16.02	15.97	14.67	13.18	12.91
20	13.38	13.39	14.60	16.12	16.11	14.78	13.32	13.00
25	13.47	13.48	14.71	16.13	16.12	14.78	13.36	12.94
30	13.49	13.42	14.67	16.05	16.12	14.71	13.27	12.89
35	13.56	13.48	14.57	16.00	16.01	14.67	13.24	12.84
40	13.47	13.42	14.38	15.86	15.95	14.64	13.21	12.78
45	13.35	13.29	14.37	15.79	15.88	14.57	13.22	12.76
50	13.30	13.20	14.35	15.73	15.74	14.51	13.11	12.74
55	13.18	13.07	14.12	15.57	15.70	14.50	13.05	12.69
60	13.14	13.01	14.05	15.49	15.71	14.43	13.04	12.60
65	13.11	12.95	14.03	15.47	15.60	14.41	13.00	12.56
70	13.07	12.88	13.93	15.35	15.56	14.38	12.96	12.57
75	13.01	12.86	13.90	15.29	15.47	14.35	12.93	12.54
80	12.96	12.80	13.85	15.27	15.41	14.32	12.88	12.49
85	12.95	12.75	13.77	15.16	15.40	14.21	12.85	12.39
90	12.84	12.66	13.70	15.11	15.36	14.24	12.86	12.40
95	12.83	12.72	13.71	15.14	15.34	14.26	12.78	12.39
100	12.91	12.77	13.95	15.37	15.43	14.41	12.87	12.46
Pressures from the lumped parameter model [mmHg]								
0	92.34	92.31	92.27	92.24	92.20	92.17	92.13	92.10
5	101.98	101.08	100.20	99.26	98.37	97.56	96.83	96.14
10	121.46	121.22	120.95	120.61	120.24	119.84	119.41	118.87
15	133.55	133.44	133.31	133.14	132.95	132.75	132.53	132.27
20	138.92	139.08	139.23	139.39	139.54	139.68	139.81	139.94
25	141.30	141.59	141.87	142.17	142.47	142.76	143.05	143.35
30	140.69	141.04	141.38	141.75	142.11	142.46	142.80	143.17
35	135.81	136.24	136.66	137.12	137.57	138.00	138.41	138.84
40	133.26	133.19	133.13	133.08	133.04	133.03	133.04	133.08
45	132.46	132.56	132.65	132.75	132.85	132.93	133.01	133.08
50	129.72	129.78	129.83	129.89	129.95	130.00	130.06	130.11
55	126.20	126.20	126.19	126.19	126.19	126.19	126.18	126.18
60	122.77	122.68	122.59	122.48	122.37	122.26	122.15	122.03
65	119.09	118.94	118.79	118.61	118.44	118.27	118.09	117.90
70	114.77	114.71	114.65	114.57	114.49	114.40	114.32	114.21
75	109.84	109.81	109.79	109.76	109.74	109.71	109.69	109.67
80	105.12	105.19	105.26	105.34	105.42	105.51	105.59	105.68
85	101.15	101.25	101.36	101.48	101.61	101.73	101.86	102.00
90	97.71	97.80	97.89	98.00	98.10	98.21	98.31	98.43
95	94.71	94.74	94.76	94.79	94.82	94.86	94.89	94.94
100	92.34	92.31	92.27	92.24	92.20	92.17	92.13	92.10

Table 1: Cross-sectional radii and pressures at the 8 cross-sections. Time is expressed in percentage with respect to the cardiac cycle (equal to 0.8 seconds), and the first and the last observations coincide due to the periodic cycle.

limited to some seconds, thus ensuring a practical clinical application of the method.

Acknowledgments

Authors acknowledge Flagship Project “Factory of the Future Fab@Hospital”, funded by Italian CNR and MIUR organisations. Michele Conti acknowledges ERC Starting Grant through the Project ISOBIO: Isogeometric Methods for Biomechanics (No. 259229).

References

- [1] Gilioli, G., Pasquali, S., Ruggeri, F. (2012). “Bayesian analysis of a stochastic predator-prey model with nonlinear functional response.” *Mathematical Biosciences and Engineering*, **9**, 75–96.
- [2] Kloeden, P.E., Platen, E. (1992). “Numerical solution of stochastic differential equations.” Springer, Berlin.
- [3] Lanzarone, E., Casagrande, G., Fumero, R., Costantino, M.L. (2009). “Integrated model of endothelial NO regulation and systemic circulation for the comparison between pulsatile and continuous perfusion.” *IEEE Transactions on Biomedical Engineering*, **56**, 1331–1340.
- [4] Lanzarone, E., Liani, P., Baselli, G., Costantino, M.L. (2007). “Model of arterial tree and peripheral control for the study of physiological and assisted circulation.” *Medical Engineering & Physics*, **29**, 542–555.
- [5] Lanzarone, E., Pasquali, S., Mussi, V., Ruggeri, F. (2014). “Bayesian estimation of thermal conductivity and temperature profile in a homogeneous mass.” *Numerical Heat Transfer - Part B*, DOI 10.1080/10407790.2014.922848.
- [6] Lanzarone, E., Ruggeri, F. (2013). “Inertance estimation in a lumped-parameter hydraulic simulator of human circulation.” *Journal of Biomechanical Engineering - T ASME*, **135**(6), 061012.
- [7] Oksendal, B. (2003). “Stochastic differential equations: an introduction with applications.” 6th Edition. Springer, Berlin.
- [8] Pearson, A.C., Guo, R., Orsinelli, D.A., Binkley, P.F., Pasierski, T.J. (1994). “Transesophageal echocardiographic assessment of the effects of age, gender, and hypertension on thoracic aortic wall size, thickness, and stiffness.” *American Heart Journal*, **128**, 344–351.
- [9] Plummer, M. (2003). “JAGS: A program for analysis of Bayesian graphical models using Gibbs sampling.” In: *Proceedings of the 3rd International Workshop on Distributed Statistical Computing*. Vienna, Austria.